Development of a small car-mounted magnetic resonance imaging system for human elbows using a 0.2 T permanent magnet

Mayu Nakagomi[1], Michiru Kajiwara[1], Jumpei Matsuzaki[1], Katsumasa Tanabe[1], Sodai Hoshiai[2], Yoshikazu Okamoto[l], and Yasuhiko Terada[1]

1 *Institute of Applied Physics, University of Tsukuba, Tsukuba, Ibaraki, Japan,*

2 *Institute of Clinical Medicine, Department of Diagnostic and Interventional Radiology, University of Tsukuba, Tsukuba, Ibaraki, Japan*

*Correspondence to: Yasuhiko Terada, Institute of Applied Physics, University of Tsukuba, Tsukuba, 1-1-1 Tennodai, Tsukuba, Ibaraki, Japan 305-8573

TEL: +81-29-853-5214, FAX: +81-29-853-5769

terada@bk.tsukuba.ac.jp

Abstract

Portable magnetic resonance imaging (MRI) scanners can provide opportunities for mobile operation in many environments including disease screening and primary care suites. Here, we develop a new, compact transportable MRI system for imaging small joints of the extremities using a 0.2 T, 200 kg permanent magnet. The whole system, including the magnet, gradient coils, RF probes, and MRI consoles (80 kg in weight) was installed in a standard-size minivan-style vehicle. The use of the open-geometry magnet enables easy patient positioning within the limited space of the vehicle. We show that our portable MRI system provides clinically relevant images of screening for elbow injuries induced by overuse of overhand throwing. This transportable system is deployable during sport events or in environments with poor access to MRI systems, and could be applicable for mass screening, early diagnosis, and case finding.

Magnetic resonance imaging (MRI) is an important diagnostic tool in clinical practice. Standard clinical MRI scanners use massive superconducting magnets with high field strength to overcome the low sensitivity of signal detection based on Faraday induction. The ever-increasing size and cost of these scanners limit their numbers on site and require doctors to create patient priority lists.

Mobile MRI systems have gained increasing attention because they allow access to MRI in resource-poor environments, without the strict siting requirements and the high costs of conventional large scanners. Mobile MRIs can be used for diagnostics in remote places and can offer medical examination for more patients.

One approach for realizing portable systems is to exploit the inhomogeneous magnetic fields to encode images spatially. The nuclear magnetic resonance mobile universal surface explorer (NMR-MOUSE) [1,2] is a transportable NMR device with a single-sided magnet, and there are numerous branches of single-sided MRI systems that are exploited with a similar concept. These systems have explored relaxing the homogeneity constraint and used the field inhomogeneity of a small magnet for spatial encoding. Based on this concept, Cooley et al. developed a series of 0.1 T, head-only portable MRI scanners with Halbach arrays of sparse cylinder magnets [3,4]. To overcome the field inhomogeneity, which is ~1000 times larger than for typical MRI magnets, they rotated the main magnet mechanically to encode the magnetic field instead of using conventional electronic gradient coil hardware.

Another approach for realizing portability is to simply use a small, homogenous magnet with a portable console and electronic devices [5,6]. For example, Kimura et al. exploited an electrically mobile MRI system with a 0.3 T, 80 mm gap magnet to diagnose diseased branches of pear trees in a research orchard [7]. Geya et al. transported a 0.2 T, 160 mm gap magnet using an electrically mobile cart to the research orchard to perform longitudinal NMR parameter measurements of growing pears [8]. Jones et al. reported on a transportable MRI for living trees using a 0.025 T, 210 mm gap magnet [9]. Small portable magnets have also been used for medical imaging applications. The MagneVu, with a permanent 0.2 T magnet [10], is a portable wrist scanner with a low field homogeneity ($T2^*$~25 μs) and a limited imaging volume. Terada et al. developed a 0.3 T, 80 mm gap wrist scanner for skeletal age examination [11]. The PoleStar N-20 is a mobile brain scanner using a 0.15 T, 27 cm gap magnet capable of imaging in an operating room [12]. Prepolarized systems also have potential for imaging extremities with portability [13,14].

There is also another type of mobile MRI system using commercial whole-body magnets installed on large trailers. They are mostly used to share costs between small healthcare facilities, and to test the viability of a full-time, fixed MRI scanner and avoid a potentially costly mistake. Although these mobile MRI trailers provide the same diagnostic performance as that of fixed whole-body scanners, they are very large and expensive, and their portability is limited.

In this work, we used a small, homogeneous magnet that is mountable on a small vehicle to realize a mobile MRI. We developed an in-vehicle MRI system with a 0.2 T permanent magnet that allows imaging of the small human joints. To validate the diagnostic performance of the portable system, we examined the detection capability for “pitcher’s elbow” injuries that occur in throwing athletes’ elbows; which is a common injury among young baseball players. Pitcher’s elbow is caused by stressful and repetitive motion of overhand throwing, resulting in pain and swelling in the elbow. Patients with pitcher’s elbow can return to play sooner if the injury is detected early and appropriately treated, and, thus, regular medical screening is quite important. The usefulness of MRI in diagnosing baseball-induced elbow injuries has been reported in several studies using both whole-body scanners at hospitals [15-19] and an extremities low-field scanner in a standard research room [20]. We show that the vehicle-mounted MRI used in this study can be applied for screening potential damage in young baseball players on baseball fields.

METHOD

Transportable MRI system

An overview of the MRI system used in this study is shown in Fig. 1. It consisted of a permanent magnet, gradient coils, a radiofrequency (RF) probe with shielding cloths, and

the MRI console. The magnet was a 0.2 T permanent magnet (NEOMAX Engineering, Japan; 200 kg; 16 cm-gap; 44 cm×50 cm×36 cm). The pole piece was 43.6 cm in diameter and 5.4 cm in height; it was made of silicon steel and stainless steel of grade SS400. The field homogeneity was nominally 50 ppm over 10 cm diameter of spherical volume (DSV), and was measured to be 7.7 ppm (root mean square) over 8 cm DSV (Supplemental Fig. S1(a)). The standard passive shimming was done by the manufacturer. The DSV of the imaging volume was 10 cm. The magnet temperature was not controlled. The field-frequency lock approach [21] was used to correct the frequency shift due to the temperature drift. The B0 drift was typically –72 Hz/min (–8.3 ppm/min) in the vehicle (Supplemental Fig. S1(b)).

The home-built RF probe consisted of a solenoid RF coil (12 turns, 130 mm long, 94 mm in diameter) and a rectangular shield box (200 mm (x)×200 mm (y)×132 mm (z)) made of 200-μm-thick brass plates. The unloaded-to-loaded Q ratio was 198/110. The bandwidth of the loaded coil (typically 79.2 kHz) was sufficiently larger than the image bandwidth (12.5 kHz). The size of the RF coil was sufficiently large to fit most of the junior baseball players. There was still available space in the gap up to 16 mm, and larger coils can be built if necessary. Conductive shielding cloths (ESD EMI Engineering Corporation, Tokyo, Japan) were attached to the RF shield box to electromagnetically shield the subject (Fig. 1(b,c)). When imaging the subject, additional shielding cloths were wound around the upper and lower arm to further reduce an external noise. The biplanar gradient coils (Fig. 1(d)) were

designed using a combined method of singular value decomposition and genetic algorithm [22]. Each gradient coil element was fabricated using printed circuit boards (PCBs) as follows. The coil-winding pattern was edited with computer-aided software, converted to a drawing exchange format, and an order was sent to an e-commerce company (p-ban.com). The company fabricated the PCBs (rigid FR4 boards including two copper layers with the thickness of 0.175 mm) according to the DXF data. Then, the *x*, *y*, and *z* PCB gradients were stacked, wired, and fixed firmly with epoxy resin. The gradient efficiencies were 1.72 (*x*), 1.72 (*y*), and 3.33 (*z*) mT/m/A. The maximum gradient strengths were 17.2 (*x*), 17.2 (*y*), and 33.3 (*z*) mT/m. The resistances were 1.1 (*x*), 1.1 (*y*), and 0.8 (*z*) Ω. The inductance values were 300 (*x*), 320 (*y*), and 24 (*z*) μH. The slew rates were 50.7 (*x*), 50.7 (*y*), and 111 (*z*) mT/m/ms. The nonlinearity of the field gradient was within 5% over 90 mm DSV. No cooling system was used for the gradient. The gradient was not actively shielded.

The MRI console consisted of a digital transceiver (DTRX6, MRTechnology, Japan), a gradient driver (20 V, 10 A, DST Inc., Japan), a preamplifier (noise figure was 0.5 dB, gain was 30 dB; DST Inc., Asaka, Japan), an active transmit/receive switch, and a transmitter (9 MHz, 150 W; DST Inc.), which were installed in a 19-inch rack (56 cm×77 cm×60 cm, 80 kg) (Fig. 1(e)).

An overview of the transportable MRI system mounted on a small vehicle (Mercedes Benz, GH-639811, width 191 cm, height 193 cm, and length 476 cm) is as follows. The

interior was 110 cm wide, 130 cm high, and 240 cm long as shown in Fig. 2. The overall weight of the system was under the maximum authorized payload and all the devices could be mounted on the vehicle. The magnet was loaded into the vehicle using a hand lift and was screwed onto an aluminum stand that was anchored to the sheet rail of the vehicle. The MRI console was loaded onto the vehicle by hand, and was tightly fixed to the front seat using ropes. All the electronic devices were operated at 100 V AC and the current needed was 10 A. A power cable was connected from the vehicle to a wall outlet on the nearest building.

Volunteer study

The image quality was evaluated through a volunteer study. The subject was positioned on a legless chair with the arm inserted into the scanner. Scout images were acquired, and the subject's position was adjusted by changing the angle of the chair's backrest. Coronal images of the normal human elbows (nine subjects, 22-44 years old) were acquired for the volunteer study. The sequence used was a gradient echo sequence. The imaging parameters are listed in Table 1. The whole measurement time for positioning the subject and imaging the right and left elbows was within 10 min. The subjects were also imaged with the same MRI system located indoors in a laboratory room.

For comparison, coronal images of the elbows of the same subjects were acquired with a stationary, commercial 0.2 T MRI (C-Scan, Esaote, Genova, Italy) that was used for

diagnosing baseball elbows [20]. The sequence used was a gradient echo sequence with the same parameters used for the portable system.

To test the clinical applicability of the portable system, the image quality was graded according to the criteria for detecting early-stage elbow injuries in baseball players. The image quality was graded by two radiologists (raters A and B) on a four-point scale: 1 = nondiagnostic, 2 = fair, 3 = good, and 4 = excellent. Raters A and B have 18 and 12 years of experience in musculoskeletal radiology, respectively. Rater A also has five years of experience in diagnosing baseball elbow.

This study was approved by the Ethics Committee of our institution. We obtained written informed consent from the study participants in all examinations.

RESULTS

Examples of MRI images

Figure 3 presents examples of MR images acquired in a laboratory setting and those acquired in the vehicle using the portable system, and image acquired with the stationary scanner. We did not use any kind of shielded room for all of the settings. The image quality scores evaluated by rater A are marked in the images. Most of the images clearly showed anatomical structures, such as the medial collateral ligament (MCL), radial, ulna, humerus,

and joint spaces. No motion artifacts were apparent in the acquired images for all of the subjects.

The mean signal-to-noise ratio (SNR) is listed in Table 2. The mean SNR for the in-vehicle measurement was almost the same as that for the indoor measurement, and they were about half of the mean SNR for the commercial scanner.

Effect of local shielding

To reject external electromagnetic noise coming into the image bandwidth, we used conductive shielding cloths: cloths attached to the RF shield box and additional cloths wrapped around the subject's arm. To measure the shielding efficiency, the elbow images were acquired with and without the additional shielding cloths wrapping the arm (Fig. 4). Without the additional cloths (Fig. 4(b)), the image showed a low SNR (3.8 for the humerus and 2.9 for the muscle), whereas with the additional cloths (Fig. 4(a)), the image exhibited a high SNR (20 for the humerus and 17 for the muscle). In this case, the reduction ratio for the external noise was 15 dB.

Image evaluation

Figure 5 shows examples of images with different rated scores. Overall, the distributions of the rated scores between the indoor and in-vehicle measurements were

similar. The scores were higher than 3 (good quality) in most cases, and no image was rated as nondiagnostic. The image shown in Fig. 5(c) was rated as “fair quality” because the MCL was hardly visible because of positioning failure, although the SNR was high, so that other anatomical structures were visible.

DISCUSSION

The magnet and console were quite small and there was sufficient room in the vehicle for the subject, thus, providing a comfortable examination environment and high-quality images without motion artifacts. The local shield using the shielding cloths largely reduced the external noise, and the image SNRs in the vehicle were almost the same as those in the indoor environment. The quality of the elbow images was good enough to visualize the anatomical features. The two raters judged the clinical diagnostic quality of the acquired images and evaluated that all the images could be used to diagnose damage of young baseball players in baseball fields.

There were several limitations in this study. First, the image SNR of the portable system was sufficient, but still low (~60% of that of the commercial scanner). Moreover, in some cases, the external noise appeared as zipper artifacts (image not shown). The signal intensity may be improved by using a quadrature coil or by averaging the signal at the cost of the increasing scan time. Many commercial low-field scanners use quadrature detection with

two orthogonal coils to improve SNR by $\sqrt{2}$. The noise level may be reduced by using an LC balun circuit [23] or sophisticated denoising techniques such as deep-residual learning [24]. Many postprocessing denoising algorithms [25,26] have been proposed and used for noise reduction.

Second, the shielding effect was not fully evaluated and room for improvement remains. The use of much larger, additional cloths would improve the shielding effect. The attainable SNR could be evaluated by performing the measurement in a shielded room, or with a dummy conducting and a dielectric arm that is completely shielded. A comparison of the noise level in a completely shielded system with that in the loaded coil would also be useful.

Third, in some cases, the subject was not adequately positioned, and, thus, the important tissues such as MCL were not clearly imaged. In this study, an untrained operator adjusted the subject's position but the positioning by a trained radiologist would reduce the positioning failure.

The portable scanner used in this study would expand the possibility of early detection of elbow injuries. Our portable scanner would also facilitate medical imaging applications in a mobile environment, including early detection of osteoarthritis and cartilage repair, disease screening during sporting events, and diagnosis of early disease of overuse injuries in sport, such as baseball, tennis, and golfer's elbow.

CONCLUSION

In this study, we developed a portable MRI system for extremities with a 0.2 T magnet. The whole system, including the magnet and MRI console, was mounted on a standard-size vehicle, and, thus, had high transportability. The quality of elbow images acquired with this system was mostly high, revealing the potential of maximizing its clinical availability to many environments.

ACKNOWLEDGMENT

The authors would like to thank Dr. Haishi for his help with mounting the system on his vehicle and Dr. Kose for his help with building the RF probe.

References

[1] G. Eidmann, R. Savelsberg, P. Blümler, B. Blümich, The NMR MOUSE, a mobile universal surface explorer, J. Magn. Reson. **122** (1996) 104–109.

[2] B. Blümich, P. Blümler, G. Eidmann, A. Guthausen, R. Haken, U. Schmitz, K. Saito, G. Zimmer, The NMR-mouse: construction, excitation, and applications, Magn. Reson. Imag. **16** (1998) 479–484.

[3] C. Z. Cooley, J. P. Stockmann, B. D. Armstrong, M. Sarracanie, M. H. Lev, M. S. Rosen, L. L. Wald, Two-dimensional imaging in a lightweight portable MRI scanner without gradient coils , Magn. Reson. Med. 73 (2015) 872-83.

[4] C. Z. Cooley, J. P Stockmann, P. C. McDaniel, C. Sappo, C. Ha, C. E. Vaughn, M. S. Rosen, T. Witzel, and L. L. Wald, Improved Uniformity of the Spatial PSF for Portable MRI Using an Optimized Rotating Magnet, Proc. 25th Annu. Meet. ISMRM Honol. 2017, p. 1049, 2017.

[5] M. Rokitta, E. Rommel, U. Zimmermann, A. Haase, Portable nuclear magnetic resonance imaging system, Rev. Sci. Instrum. 71 (2000) 4257–4262.

[6] F. Okada, S. Handa, S. Tomiha, K. Ohya, K. Kose, T. Haishi, S. Utsuzawa, K. Togashi, Development of a portable MRI for outdoor measurements of plants, in: The Sixth Colloquium on Mobile Magnetic Resonance, Aachen, Germany, 6–8 September, 2006.

[7] T. Kimura, Y. Geya, Y. Terada, K. Kose, T. Haishi, H. Gemma, Y. Sekozawa, Development of a mobile magnetic resonance imaging system for outdoor tree measurements, Rev. Sci. Instrum. **82** (2011) 053704.

[8] Y. Geya, T. Kimura, H. Fujisaki, Y. Terada, K. Kose, T. Haishi, H. Gemma, Y. Sekozawa, Longitudinal NMR parameter measurements of Japanese pear fruit during the growing process using a mobile magnetic resonance imaging system, J. Magn. Reson. **226** (2013) 44–51.

[9] M. Jones, P.S. Aptaker, J. Cox, B.A. Gardiner, P.J. McDonald, A transportable magnetic resonance imaging system for in situ measurements of living trees: the Tree Hugger, J. Magn. Reson. 218 (2012) 133–140.

[10] G. Gold , D. Theodorou, T. Blair, G. Garcia, C. Crowley, F. Rose, D. Trudell , D. Resnick, MR imaging of the wrist with a portable extremity scanner. In: Proc 19th Annual Meeting ISMRM, Philadelphia; 1999. p 2039.

[11] Y. Terada, K. Ishizawa, S. Inamura, K. Kose, Development of a Portable Wrist MRI for Skeletal Age Assessment, In: Proc 21th Annual Meeting ISMRM, Salt Lake City; 2013. p 2761.

[12] V. Ntoukas, R. Krishnan, V. Seifert, The New Generation Polestar N20 for Conventional Neurosurgical Operating Rooms: a Preliminary Report, Neurosurgery. **62** (2008) 82-9.

[13] A. Macovski. MRI: A charmed past and an exciting future. J Magn Reson Imaging **30** (2009) 919–923.

[14] I. Savukov, T. Karaulanov, A. Castro, P. Volegov, A. Matlashov, A. Urbatis, J. Gomez, M. Espy. Non-cryogenic anatomical imaging in ultra-low field regime; Hand MRI demonstration. J Magn Reson. **211** (2011) 101–108.

[15] J.P. Salvo, L. Rizio, J.E. Zvijac, J.W. Uribe, K.S. Hechtman. Avulsion fracture of the ulnar sublime tubercle in overhead throwing athletes. Am J Sports Med. **30** (2002) 426–31.

[16] L.S. Steinbach, R.C. Fritz, P.F. Tirman, M. Uffman. Magnetic resonance imaging of the elbow. Eur J Radiol. **25** (1997) 223–41.

[17] M. J. Tuite, R. Kijowski. Sports-related injuries of the elbow: an approach to MRI interpretation. Clin Sports Med. **25** (2006) 387–408.

[18] F. Del Grande, M. Aro, S. J. Farahani, J. Wilckens, A. Cosgarea, J. A. Carrino. Three-Tesla MR imaging of the elbow in non-symptomatic professional baseball pitchers. Skelet Radiol. **44** (2015) 115–23.

[19] A. S. Wei, S. Khana, O. Limpisvasti, J. Crues, L. Podesta, L. A. Yocum. Clinical and magnetic resonance imaging findings associated with little league elbow. J Pediatr Orthop. **30** (2010) 715–9.

[20] Y. Okamoto, K. Maehara, T. Kanahori, T. Takashi Hiyama, T. Kawamura, M. Minami, Incidence of elbow injuries in adolescent baseball players: screening by a low field magnetic resonance imaging system specialized for small joints , Jpn. J. Radiol. **34** (2016) 300-6.

[21] S. Handa, H. Yoshioka, S. Tomiha, T. Haishi, and K. Katsumi, Optimized system design and construction of a compact whole-hand scanner for diagnosis of rheumatoid arthritis, Magn. Reson. Med. Sci. **6** (2007) 113–120.

[22] K. Matsuzawa, K. Kose, Y. Terada, A new method for optimizing performances of gradient coils based on singular value decomposition and genetic algorithm, In: Proc 25th Annual Meeting ISMRM, Honolulu; 2017. p 4337.

[23] S. Handa, T. Haishi, K. Kose, Development of a local electromagnetic shielding for an extremity magnetic resonance imaging system, Rev. Sci. Instrum. **79** (2008) 113706.[24] K. Zhang, W. Zuo, Y. Chen, D. Meng, L. Zhang, Beyond a Gaussian Denoiser: Residual Learning of Deep CNN for Image Denoising, IEEE Trans. Imag. Processing 26 (2017) 3142-3155.

[25] J. Mohan, V. Krishnaveni, Y. Guo, A survey on the magnetic resonance image denoising methods, Biomedical Signal Processing and Control **9** (2014) 56-69.

[26] D. Ai, J. Yang, J. Fan, W. Cong, X. Wang, Denosing filters evaluation for magnetic resonance images, Optik **126** (2015) 3844-3850.

Figure captions

Fig. 1 Overview of the MRI system. (a,b) Schematic (a) and photo (b) of the RF probe, gradient coils, and magnet; (c) RF probe and shielding cloths; (d) overhead views of the PCB-gradient coils (left) and their winding patterns (right); (e) MRI console.

Fig. 2 Overview of the transportable MRI system. (a) Overview of the vehicle; (b) 3D-schematic of the system; (c) back view of the magnet and the stand; (d) front view of the magnet and the console; (e) volunteer study.

Fig. 3 Coronal images of the elbows of (a) a 22-year-old male and (b) a 24-year-old male. The image quality rated by rater A is also shown.

Fig. 4 Evaluation of shielding efficiency. (a) Measurement with the additional shielding cloths; (b) measurement without the additional shielding cloths. The yellow, blue, and red squares in the MR images correspond to regions of interest of the humerus, muscle, and outside area.

Fig. 5 (a,b) Image scores rated by rater A (a) and rater B (b); (c-e) examples of images rated as (c) fair, (d) good, and (e) excellent.

Table 1 Imaging parameters

Parameter	Value
Repetition time/echo time (ms)	500/16
Flip angle (°)	75
Slice thickness (ms)	3
Number of slices	9
Matrix size	256×192
Field of view (mm^2)	180×180
Measurement time	1 min 36 s
Bandwidth (kHz)	12.5
Dwell time (μs)	80
Readout window length (ms)	20.48

Table 2 Mean signal-to-noise ratio

	Muscle	Humerus
Indoor	16.6	21.8
In-vehicle	17.0	20.7
Commercial scanner	29.7	30.5

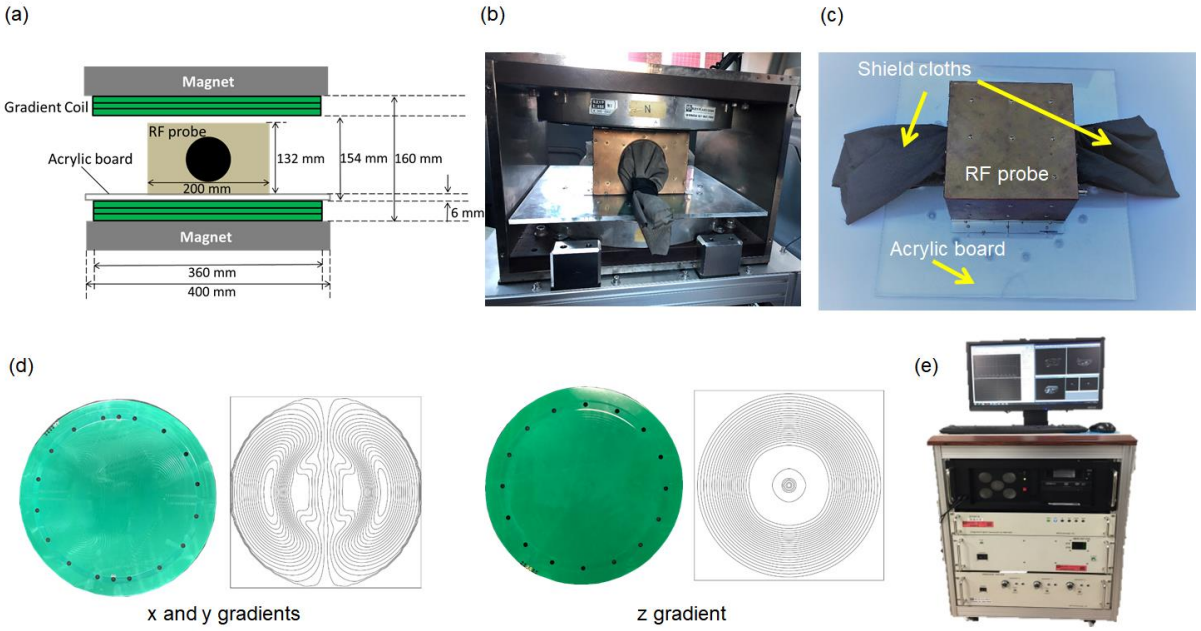
(a)
Magnet
Gradient Coil
RF probe
Acrylic board
132 mm
154 mm
160 mm
200 mm
6 mm
Magnet
360 mm
400 mm
(b)
(c)
Shield cloths
RF probe
Acrylic board
(d)
x and y gradients
z gradient
(e)

Fig. 1

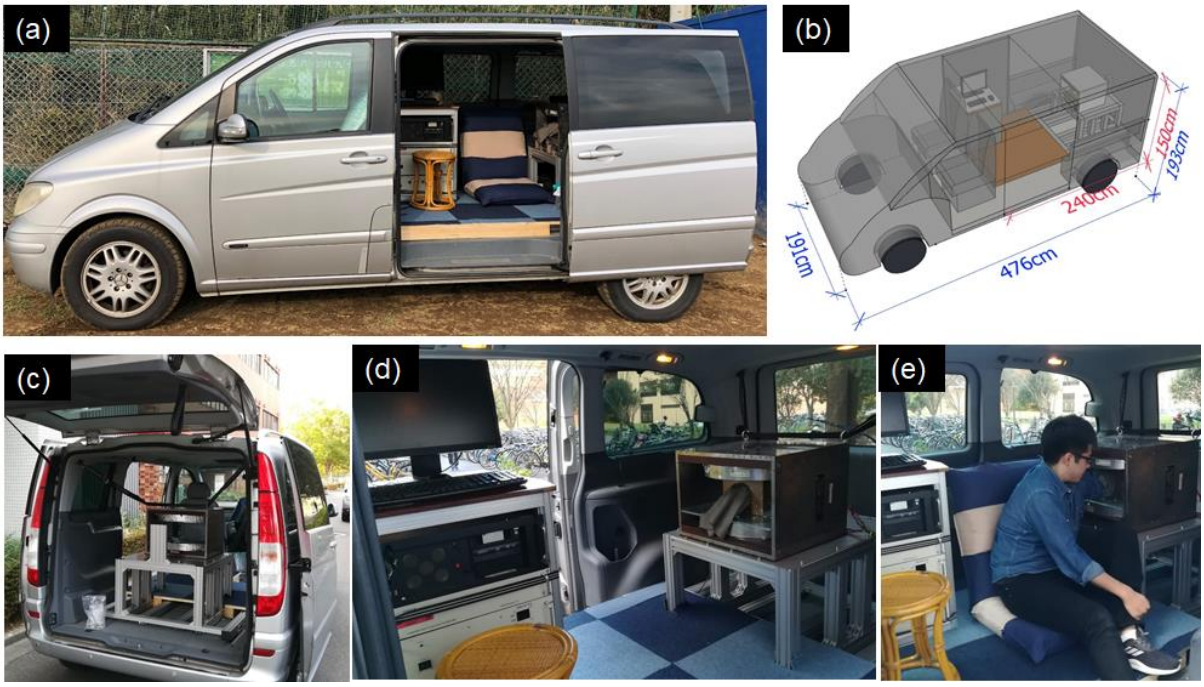

Fig. 2

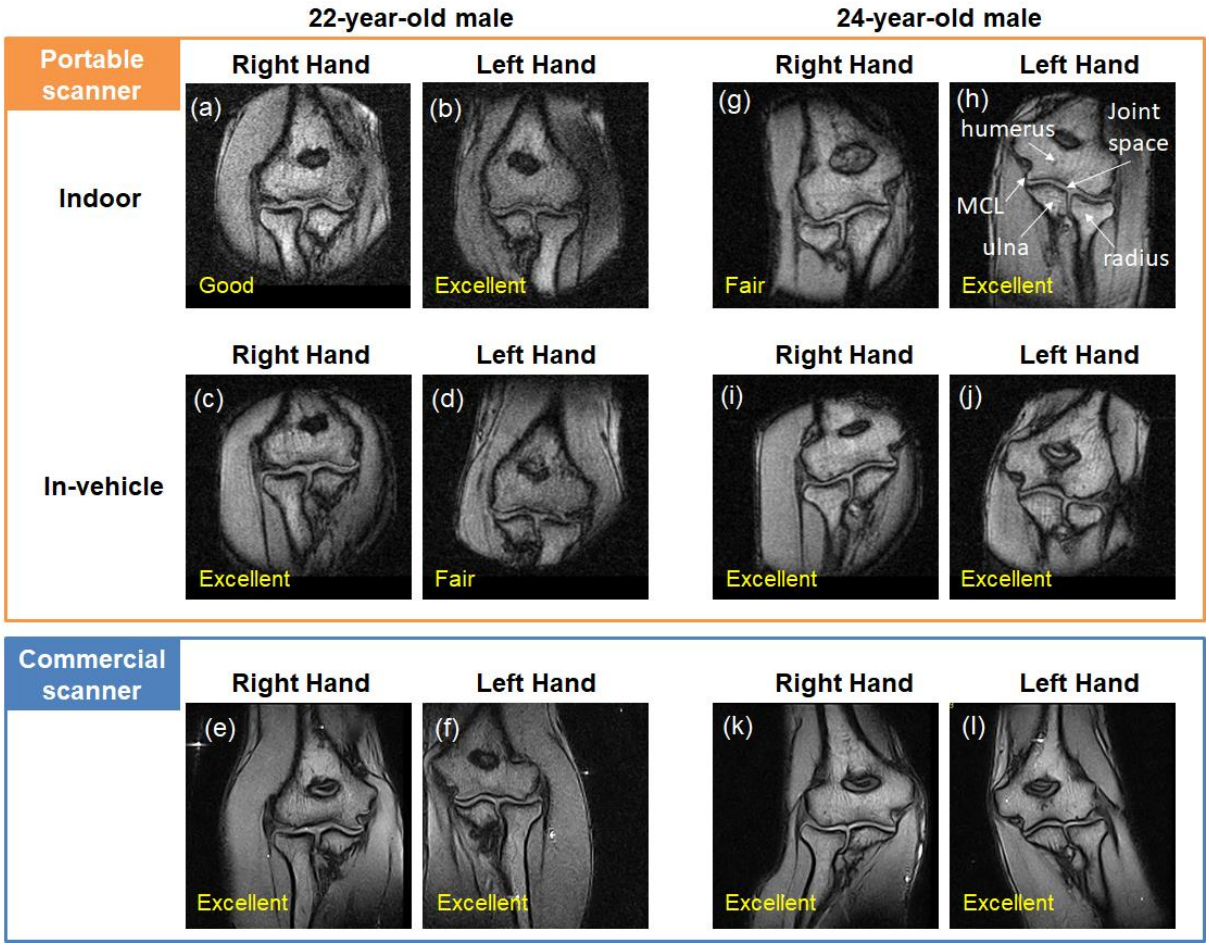
22-year-old male
24-year-old male
Portable scanner
Indoor
In-vehicle
Commercial scanner
Right Hand
Left Hand
(a)
Good
(b)
Excellent
(g)
Fair
(h)
humerus
Joint space
MCL
ulna
radius
Excellent
(c)
Excellent
(d)
Fair
(i)
Excellent
(j)
Excellent
(e)
Excellent
(f)
Excellent
(k)
Excellent
(l)
Excellent

Fig. 3

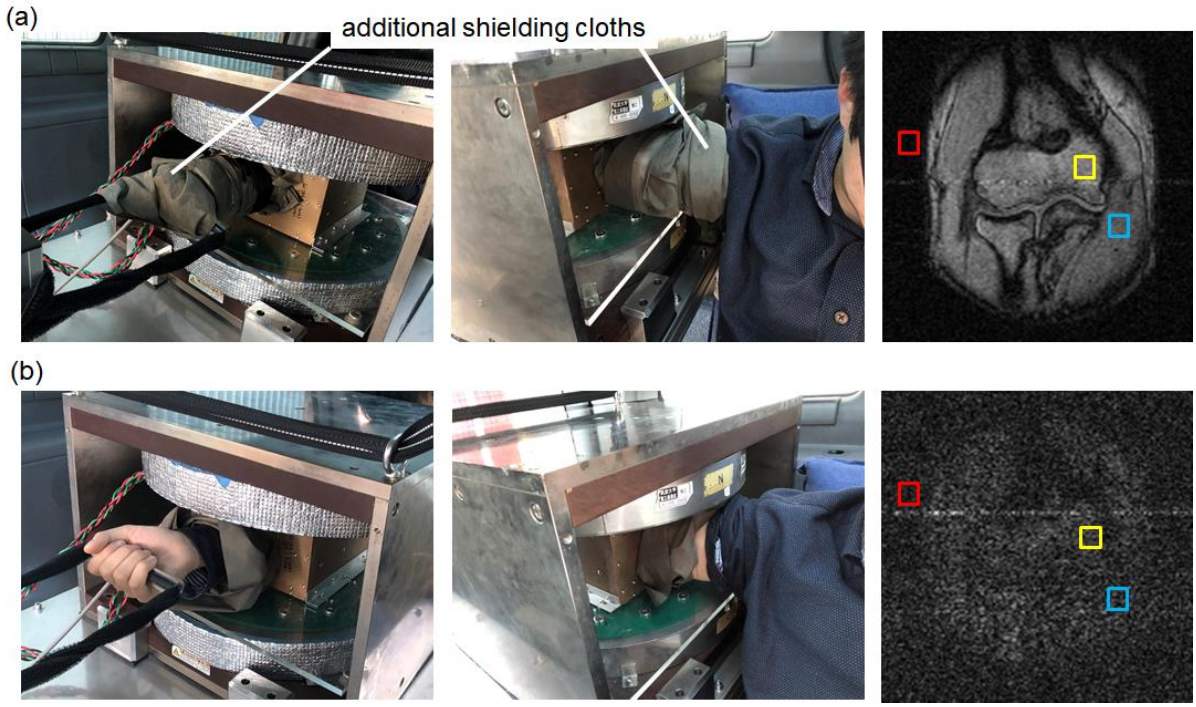

Fig. 4

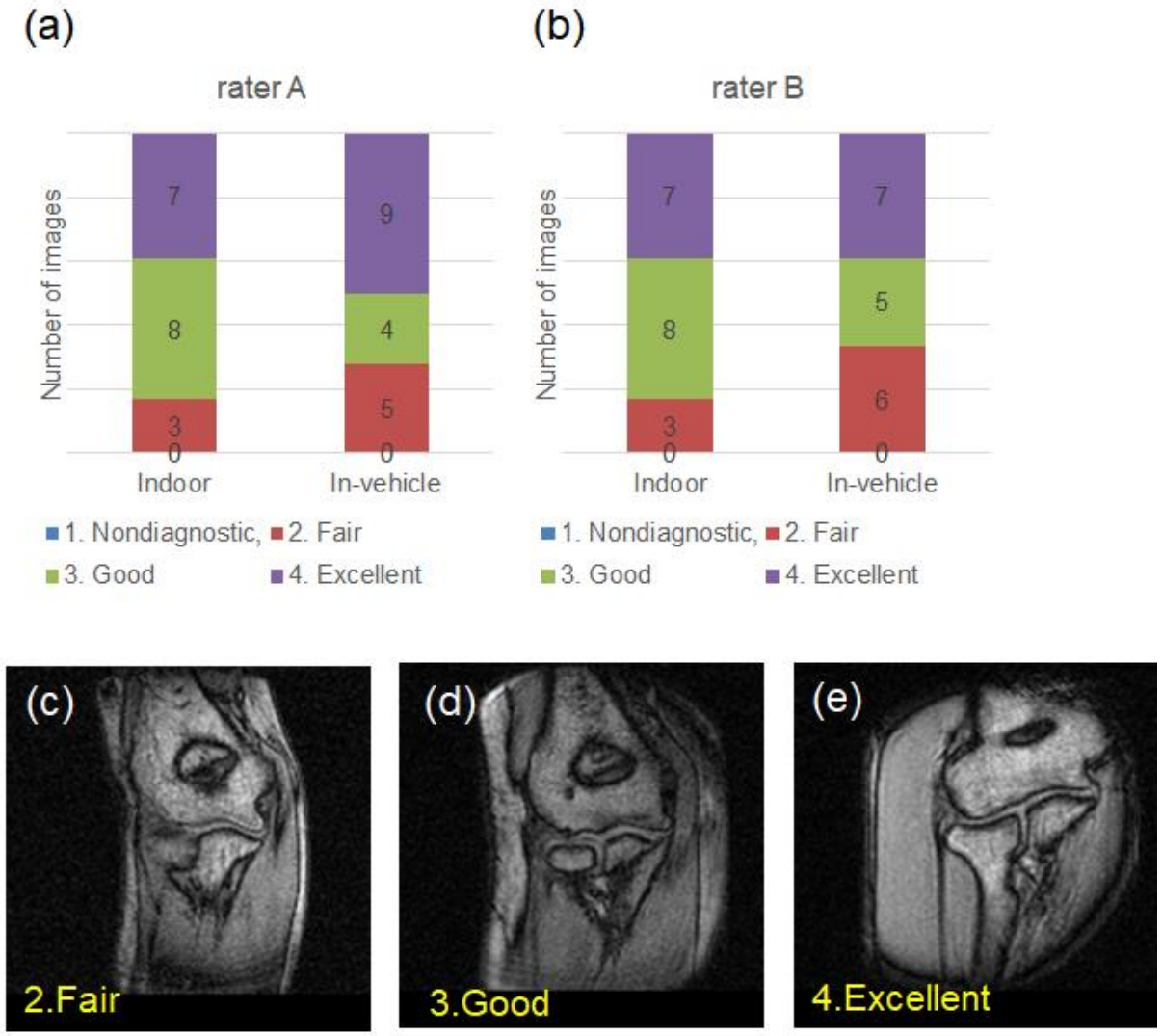
(a)
rater A
Number of images
7
8
3
0
9
4
5
0
Indoor
In-vehicle
1. Nondiagnostic,
2. Fair
3. Good
4. Excellent
(b)
rater B
Number of images
7
8
3
0
7
5
6
0
Indoor
In-vehicle
1. Nondiagnostic,
2. Fair
3. Good
4. Excellent
(c)
2.Fair
(d)
3.Good
(e)
4.Excellent

Fig. 5